AIAA JOURNAL
Vol. 46, No. 4, April 2008

Aerothermoelastic Stability of Composite Aerovehicle Wings Subjected to Heat Inputs

Gian Mario Polli* and Franco Mastroddi†
Universit of Rome "La Sapienza," 00184 Rome, Italy
Liviu Librescu‡
Virginia Polytechnic Institute and State University, Blacksburg, Virginia 24061-0219
and
Claudia Di Trapani§
Avio Propulsione Aerospaziale, 00034 Colleferro, Italy

DOI: 10.2514/1.32397

In this paper, a coupled aerothermoelastic dynamic stability analysis of composite aerovehicle wings featuring nonclassical effects, and immersed in an incompressible gas flow is developed. Specifically, the study concerns the aerothermoelastic stability of swept wings made of advanced composite materials and exposed to a heat flow generated by a laser beam impacting its deformed surface. Because of its exceptional features in thermal insulation of aerospace structures, the pyrolytic graphite is adopted in the actual numerical simulations together with consideration of a rectangular single-layered swept wing. The evaluation of the temperature field on the deformed (actual) configuration of the wing permits the authors to address the problems of the aerothermoelastic response and stability in a coupled framework. As a result, the exact analytical expression of the aerothermoelastic response of the heated wing is obtained in the Laplace space domain and, following it, the static and dynamic aeroelastic instabilities are determined. The obtained results indicate that the aeroelastic stability is substantially affected by the thermoelastic coupling. In the presentation and discussion of the results, special attention is given to the effects played by the flight speed, thermal anisotropy of the material constituent, ratio of the characteristic thermal time to the natural period of vibration, and direction of the external heat flux impacting the wing surface.

Nomenclature

A, B, C, D, E, F, G	=	aerodynamic matrices
a	=	dimensionless position of elastic axis, x_0/b
$\mathcal{A}$	=	wing cross-sectional area
$B_{ij}^{(m,n)}$, $F_i^{(m,n)}$, $I^{(m,n)}$, $S_{ij}^{(m,n)}$	=	generalized stiffness, force, mass, and stress quantities of order (m, n)
b, l	=	semichord and semispan, respectively, m
$\boldsymbol{c}$	=	vector of natural boundary conditions
C_1, C_2, D	=	geometric moments of inertia
c_t	=	specific heat
$\boldsymbol{e}_i$	=	Cartesian-based vectors
$\boldsymbol{f}$	=	load vector
g, h, θ, β	=	warping, m^{-1}, plunge, m, twist angle, and wing-section rotation displacement variables
H	=	wing thickness, m
$\tilde{\mathrm{H}}$	=	aeroelastic operator matrix
K, L, M, P	=	stiffness matrices
k_1, k_3	=	thermal conductivities in the plane of isotropy and normal to it, respectively
$\mathcal{L}$, $\mathcal{M}$	=	sectional aerodynamic lift and moment
p, s	=	Laplace transform variables associated to their physical counterparts, x_2 and t, respectively
$\boldsymbol{q}$	=	heat density vector, W/m^2
R	=	shear flexibility ratio
R, S	=	boundary-condition matrices
T	=	temperature field, K
t	=	dimensional time variables, s
x_i	=	Cartesian coordinates, $i = 1, 2, 3$
$\boldsymbol{y}$	=	displacement vector
δ_1	=	tracer identifying warping effects
Λ	=	wing sweep angle
λ_{lmn}, $\phi_{lmn}(\mathbf{x})$	=	eigenvalues and eigenfunctions of the Laplacian operator related to the temperature field in the body
ρ, ρ_∞	=	material and air density, kg/m^3
$\varphi(t)$	=	Wagner function
ω_{1_b}, ω_{1_t}	=	first bending and first torsion natural frequencies, rad/s

This paper is dedicated to the memory of Liviu Librescu who died dramatically on 16 April 2007 while on duty. He was teaching class when the mass shootings occurred at the Engineering Science and Mechanics Department, Virginia Polytechnic Institute and State University. Liviu Librescu was a very fine, caring person, unforgettable friend, outstanding academician, and an inspiring graduate research advisor. Fond memories of him shall be cherished and will continue to inspire.

Presented as Paper 1731 at the 47th AIAA/ASME/ASCE/AHS/ASC Structures, Structural Dynamics, and Materials Conference, Newport, RI, 1–4 May 2006; received 28 May 2007; revision received 27 September 2007; accepted for publication 20 November 2007.

*Research Assistant, Department of Aerospace and Astronautical Engineering, Via Eudossiana, 16.
†Professor, Department of Aerospace and Astronautical Engineering.
‡Professor, Department of Engineering Science and Mechanics.
§Aerospace Engineer, Corso Garibaldi, 22, Colleferro.

Subscripts

A	=	aerodynamic load
T	=	thermal load
M	=	mechanical external loads
$(\bullet)_c$, $(\bullet)_{nc}$	=	circulatory and noncirculatory counterparts of $(\bullet)$
$(\bullet)_n$	=	quantity $(\bullet)$ normal to the leading edge

Symbols

$\tilde{f}(x_2, s)$, $\hat{f}(p, t)$, $\tilde{\hat{f}}(p, s)$	=	Laplace transform of $f(x_2, t)$, with respect to time, space variable x_2, and with respect to both variables, respectively
∂	=	domain boundary
$\dot{}$	=	overdot, derivative with respect to time
$'$	=	prime, derivative with respect to x_2

I. Introduction

THE recent activities related to space exploration and the resurrected interest in supersonic/hypersonic flight vehicles [1–4] require a good understanding of the aeroelastic instability and response of aeronautical/aerospace flight vehicle structures operating in a high-temperature field. Although the thermoelastic dynamic response and stability of trusses and beam structures (motivated by the experience in space flight applications) have been widely investigated [5–10], to the authors' best knowledge, these theoretical analyses have never been extended to the consideration of aeronautical structures immersed in a flowfield. Nonetheless, the importance of the aerothermoelastic response and stability analyses of aerospace systems has been largely recognized [11] (especially with respect to reusable launch vehicles), and, in this sense, a number of studies have been conducted to investigate the aerothermoelastic stability of aerospace vehicles by using computational fluid dynamics (CFD) approaches for the aerodynamics and finite element (FE) models for the structures [1–4]. In this context, to the authors' best knowledge, this study presents, for the first time, an exact coupled aerothermoelastic stability analysis of heated composite aircraft wings featuring nonclassical effects. In particular, in this paper, the study of the aerothermoelastic stability of aerovehicle swept wings made of advanced composite materials, exposed to a generic heat flowfield, and operating in an incompressible flow is addressed; the thermal field is supposed to be generated by a laser beam impacting the upper surface of the wing [12], whereas the wing structural model, previously developed by the authors [12–14], is specialized to the case of a rectangular single-layered swept wing composed of a transversely isotropic material. Because of its exceptional features in thermal protection of aerospace structures [15,16], the pyrolytic graphite is adopted in the applications. One should remark that, due to the special character of the considered thermal field, a time-domain formulation of the theory of lifting surfaces was considered to be mandatory [17,18]. Moreover, the evaluation of the temperature field on the deformed (actual) configuration of the wing permits the authors to address the problem of the aerothermoelastic response and stability in a coupled framework (see [12] for a presentation of a similar analysis in an uncoupled regime). As a result, the exact analytical expression of the aerothermoelastic response of the heated aerovehicle wing is obtained in the Laplace transformed space and, consequently, the static/dynamic stability boundary of the wing model is derived. To validate the results obtained in terms of aerothermoelastic flutter boundary, the thermoelastic static and dynamic stability analysis is presented. The corresponding results are then compared with those available in literature [6–9], which are confined to the study of trusses in space subjected to solar radiant heating and solved using an approximate mathematical approach. Finally, the aerothermoelastic stability analysis is presented and the corresponding results are qualitatively compared with those available in literature which concern the aerothermoelastic stability of wings [1–4]. In the presentation and discussion of the results, particular emphasis is placed on the effects of flight speed, thermal anisotropy, ratio of the characteristic thermal time to the natural period of vibration [5], and direction of the external heat flux impacting the wing surface.

II. Structural and Aeroelastic Model

The wing structure is modeled as a platelike body with appropriate internal constraints. Specifically, it is assumed that the wing cross sections are not deformable and that the wall thickness is inextensible. As a result, the displacement field of the wing is represented by the following map [13,14]:

$$\begin{aligned}\mathbf{u}(x_1, x_2, x_3, t) =& x_3\theta(x_2, t)\boldsymbol{e}_1 - \{x_3[\beta(x_2, t) + \delta_1 x_1 g(x_2, t)]\}\boldsymbol{e}_2 \\ &+ \{h(x_2, t) - [x_1 - x_0(x_2, t)]\theta(x_2, t)\}\boldsymbol{e}_3 \end{aligned} \tag{1}$$

where $\theta(x_2, t)$ denotes the twist angle of the wing about its pitching axis, $\beta(x_2, t)$ identifies the flexural angle about the chordwise direction, $g(x_2, t)$ represents the warping displacement, $h(x_2, t)$ denotes the plunging displacement of the wing cross section measured at the elastic axis [positive upward and located at $x_{1e} = x_0(x_2)$, (Fig. 1)], δ_1 is a tracer identifying the warping effect [13], and $\boldsymbol{e}_i$ are the unit vectors in the x_i directions. The tracer takes the value of one or zero according to whether the warping inhibition is incorporated or discarded, respectively: the two resulting formulations are denoted in the following as "free warping" (FW) and "warping restraint" (WR) models, respectively. Collecting the independent displacement components in Eq. (1), one may observe that the total number of unknowns retained into the model is four, and in terms of these four displacement unknowns (β, g, θ, h) the aeroelastic response analysis under the effect of a thermomechanical load is investigated.

To be reasonably self-contained, the equilibrium equations and the related boundary conditions for a transversely isotropic swept wing, obtained via the application of Hamilton's principle, are shortly reviewed (the interested reader is referred to [12–14] for a complete presentation of this model). Specifically, denoting by $\boldsymbol{y}$ $(=\{\beta, g, \theta, h\})$ the vector of the displacement unknowns, with K, L, P the stiffness matrices including the typical stiffness parameters of a bending beam structure as indicated in details in [19], and with M the mass matrix (their expressions are supplied in [12,19], the equilibrium equations may be written in condensed form as

$$\mathrm{K}\,\boldsymbol{y}'' + \mathrm{L}\boldsymbol{y}' + \mathrm{P}\boldsymbol{y} + \mathrm{M}\ddot{\boldsymbol{y}} = \boldsymbol{f}^A + \boldsymbol{f}^T + \boldsymbol{f}^M \tag{2}$$

Herein, the primes and the overdots denote derivatives with respect to the spanwise coordinate x_2 and time t, respectively, whereas $\boldsymbol{f}^A$ is the vector of aerodynamic loads, $\boldsymbol{f}^T$ is the vector of thermal loads introduced by means of the constitutive equations, and $\boldsymbol{f}^M$ is the vector of the generic time-dependent external loads that can act during the operational life of the vehicle (e.g., explosive blast, sonic boom, gusts, etc.). The aerodynamic load vector considered in the

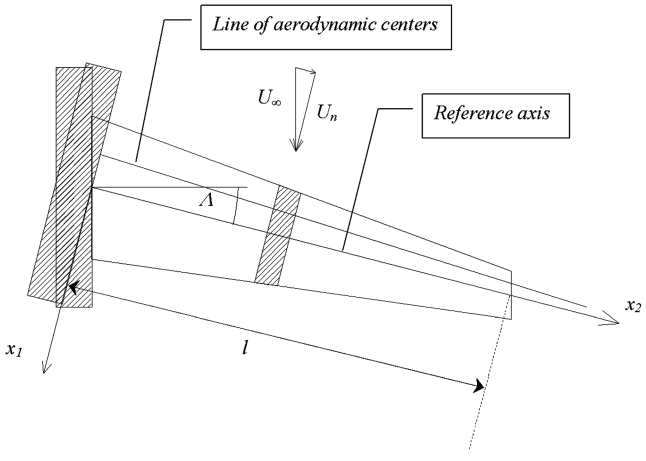

Fig. 1 Geometry of the swept wing.

analyses is based on an incompressible unsteady aerodynamic model which takes into account the effect of the sweep angle. It can be written in the following compact form [12,19,20]:

$$\boldsymbol{f}^A(\boldsymbol{y}, \dot{\boldsymbol{y}}, \ddot{\boldsymbol{y}}, \boldsymbol{y}', \dot{\boldsymbol{y}}', t, x_2) = \begin{Bmatrix} 0 \\ 0 \\ \mathcal{M} \\ \mathcal{L} \end{Bmatrix} = \mathrm{A}\ddot{\boldsymbol{y}} + \mathrm{B}\dot{\boldsymbol{y}} + \mathrm{C}\boldsymbol{y}' + \mathrm{D}\dot{\boldsymbol{y}}' + \mathrm{E}\int_0^t \varphi(t-\hat{t})\ddot{\boldsymbol{y}}(\hat{t})\,\mathrm{d}\hat{t} + \mathrm{F}\int_0^t \varphi(t-\hat{t})\dot{\boldsymbol{y}}(\hat{t})\,\mathrm{d}\hat{t} + \mathrm{G}\int_0^t \varphi(t-\hat{t})\dot{\boldsymbol{y}}'(\hat{t})\,\mathrm{d}\hat{t} \tag{3}$$

where $\mathcal{L}$ and $\mathcal{M}$ are the sectional lift and aerodynamic torque about the reference axis per unit span, $\varphi(t)$ is the Wagner's function [17,18], and A, B, C, D, E, F, G are the matrices of the aerodynamic coefficients whose expressions are provided in [12,19]. The functional representation of the vector of thermal loads will be supplied in the following section and, in particular, the explicit dependence of this load vector in terms of the unknown displacements. For the moment, let us note that using the Hooke–Duhamel constitutive equations, modified in the usual way, (e.g., [13]), and assuming a rectangular cross section for the wing, with L, c, and H denoting, respectively, the wing midspan, chord, and thickness, assumed to be constant, the vector of thermal loads has only one nonzero component which does work on the flexural deflection of the wing $\beta(x_2, t)$, namely,

$$\boldsymbol{f}^T(x_2, t) = \begin{bmatrix} \Theta'(x_2, t) \\ 0 \\ 0 \\ 0 \end{bmatrix} \tag{4}$$

where $\Theta(x_2, t)$ is the thermal moment. Specifically, the thermal moment is given in terms of the difference between the reference and the actual temperature, and due to the application of the heat flux on the upper surface

$$\Theta(x_2, t) = \int_{-c/2}^{c/2}\int_{-H/2}^{H/2} x_3\hat{\alpha}\Delta T(x_1, x_2, x_3, t)\,\mathrm{d}x_3\,\mathrm{d}x_1 \tag{5}$$

where $\hat{\alpha}$ $[=E\alpha/(1-\nu)]$ is the transformed thermal expansion coefficient. For the forthcoming developments, it is convenient to define the vector of thermal moments as the derivative of a vector $\boldsymbol{c}$ as follows:

$$\boldsymbol{f}^T(x_2, t) = \boldsymbol{c}'(x_2, t) \tag{6}$$

As a result, the boundary conditions at the root and the natural boundary conditions at the tip may be written as

$$\boldsymbol{y}(0, t) = 0 \tag{7}$$

$$\mathrm{R}\,\boldsymbol{y}'(L, t) + \mathrm{S}\boldsymbol{y}(L, t) = \boldsymbol{c}(t) \tag{8}$$

where the boundary load $\boldsymbol{c}$ reduces in our applications to a concentrated thermal moment acting on the flexural deflection of the wing:

$$\boldsymbol{c}(t) = \begin{bmatrix} \Theta(L, t) \\ 0 \\ 0 \\ 0 \end{bmatrix} \tag{9}$$

The vectorial Eq. (2) involves a system of four differential equations in space and time of the second order, whose boundary conditions are represented by Eqs. (7) and (8). To render the thermal load vector $\boldsymbol{f}^T$ dependent on the displacement vector $\boldsymbol{y}$ and on its derivatives, in a way similar to that of the aerodynamic load vector, see Eq. (3), the thermal field has to be evaluated in the deformed configuration of the wing. This idea is carried out in the following section.

III. Thermomechanical Model

As already stated, the present formulation is carried out in the framework of coupled thermoelasticity, in the sense that the temperature distribution is supposed to be affected by the actual deformation of the structure. Moreover, it is assumed that the external heat input is generated by a laser beam impacting the upper surface of the wing, and finally the wing is treated as a solid parallelepiped. Mathematically, the problem may be stated in terms of the following system of equations [5,12,19,21–23]:

$$\mathrm{Div}\,(\mathrm{K}\nabla T) - \rho c_t\frac{\partial T}{\partial t} = 0 \quad \text{for } \boldsymbol{x} \in \mathcal{B}, t \in \mathcal{T} \tag{10}$$

$$\mathrm{K}\,\nabla T \cdot \boldsymbol{n} = \boldsymbol{q} \cdot \boldsymbol{n} \quad \text{for } \boldsymbol{x} \in \mathcal{S}_U, t \in \mathcal{T} \tag{11}$$

$$\nabla T \cdot \boldsymbol{n} = 0 \quad \text{for } \boldsymbol{x} \in \partial\mathcal{B}/\mathcal{S}_U, t \in \mathcal{T} \tag{12}$$

$$T = 0 \quad \text{for } \boldsymbol{x} \in \partial\mathcal{B}, t = 0 \tag{13}$$

where $T(\boldsymbol{x}, t)$ is the temperature field, K is the thermal conductivity tensor [24], ρ is the volume density, c_t is the specific heat, $\boldsymbol{n}$ is the external normal to the surface body, and $\boldsymbol{q}$ is the external heat flux impacting the wing, $\mathcal{B}$ $(=\{(x_1, x_2, x_3)\| - c/2 \le x_1 \le c/2; 0 \le x_2 \le L; -H/2 \le x_3 \le H/2\})$ and $\mathcal{T}$ $(=\{t\|0 \le t < \infty\})$ denote, respectively, the space and time domains, and $\mathcal{S}_U$ $(=\{(x_1, x_2, x_3)\| - c/2 \le x_1 \le c/2; 0 \le x_2 \le L; x_3 = H/2\})$ denotes the upper surface of the wing where the heat input applies. For the present case of the transversely isotropic material, the thermal conductivity tensor assumes the form

$$\mathrm{K} = \begin{pmatrix} k_1 & 0 & 0 \\ 0 & k_1 & 0 \\ 0 & 0 & k_3 \end{pmatrix} \tag{14}$$

Using a Green's function approach to solve the previous system of differential equations, one obtains the following expression for the temperature field inside the wing domain [12,19]:

$$T(\boldsymbol{x}, t) = \sum_{l,m,n=0}^{\infty}\frac{\phi_{lmn}(\boldsymbol{x})}{\rho c_t}\int_{\mathcal{S}_U}\phi_{lmn}(\boldsymbol{x}^*)\int_0^t e^{-\frac{k_1\lambda_{lmn}}{\rho c_t}(t-t^*)}\boldsymbol{q}(\boldsymbol{x}^*, t^*) \cdot \boldsymbol{n}(\boldsymbol{x}^*, t^*)\,\mathrm{d}t^*\,\mathrm{d}\mathcal{S} \tag{15}$$

where

$$\phi_{lmn}\left(= -\sqrt{8\sqrt{k_3}/(\sqrt{k_1}cLH)}\cos\left[\frac{l\pi}{c}\left(x_1 + \frac{c}{2}\right)\right] \times \cos\left(\frac{m\pi}{L}x_2\right)\cos\left[\frac{n\pi}{H}\left(x_3 + \frac{H}{2}\right)\right]\right)$$

are the eigenfunctions, and $\lambda_{lmn}[= -(l\pi/c)^2 + (m\pi/L)^2 + (n\pi/\sqrt{k_1/k_3}H)^2]$ are the corresponding eigenvalues of the harmonic adjoint operator associated with the problem under consideration, whereas the superscript $*$ denotes the time and space coordinates where the impulse is applied in the Green's function approach. Using the previous equation, one can establish an explicit relationship between the temperature field and the unknown displacement components. To this end, we recall the fact that the unit vector normal to the deformed upper surface of the wing is expressed in a linear approximation as [12,19]

$$\boldsymbol{n}(\boldsymbol{x}, t) \cong \boldsymbol{e}_3 - h'(x_2, t)\boldsymbol{e}_2 + \theta(x_2, t)\boldsymbol{e}_1 \tag{16}$$

As a result, representing the heat flux vector in terms of its

components on the chosen Cartesian reference system (i.e., $\boldsymbol{q}(\boldsymbol{x},t)=\{q_1(\boldsymbol{x},t),q_2(\boldsymbol{x},t),q_3(\boldsymbol{x},t)\}$), the temperature field may be written as the sum of three terms. The first term, $T_1(\boldsymbol{x},t)$, depends on the actual pitch displacement $\theta(x_2,t)$ of the wing, and its expression is given by

$$T_1(\boldsymbol{x},t)=\sum_{l,m,n=0}^{\infty}\frac{\phi_{lmn}(\boldsymbol{x})}{\rho c_t}\times\int_{\mathcal{S}_U}\phi_{lmn}(\boldsymbol{x}^*)\int_0^t e^{-\frac{k_1\lambda_{lmn}}{\rho c_t}(t-t^*)}q_1(\boldsymbol{x}^*,t^*)\theta(x_2^*,t^*)\,\mathrm{d}t^*\,\mathrm{d}\mathcal{S} \tag{17}$$

where q_1 is the component of the heat density vector $\boldsymbol{q}$ in the chordwise x_1 direction.

The second term, $T_2(\boldsymbol{x},t)$, depends on the actual bending of the wing $[h'(x_2,t)]$, and its expression is given by

$$T_2(\boldsymbol{x},t)=-\sum_{l,m,n=0}^{\infty}\frac{\phi_{lmn}(\boldsymbol{x})}{\rho c_t}\times\int_{\mathcal{S}_U}\phi_{lmn}(\boldsymbol{x}^*)\int_0^t e^{-\frac{k_1\lambda_{lmn}}{\rho c_t}(t-t^*)}q_2(\boldsymbol{x}^*,t^*)h'(x_2^*,t^*)\,\mathrm{d}t^*\,\mathrm{d}\mathcal{S} \tag{18}$$

where q_2 is the component of the heat density vector $\boldsymbol{q}$ in the spanwise x_2 direction.

The third term, $T_3(\boldsymbol{x},t)$, does not depend on the displacement vector and represents the uncoupled temperature field considered in [12], and its expression is

$$T_3(\boldsymbol{x},t)=\sum_{l,m,n=0}^{\infty}\frac{\phi_{lmn}(\boldsymbol{x})}{\rho c_t}\int_{\mathcal{S}_U}\phi_{lmn}(\boldsymbol{x}^*)\int_0^t e^{-\frac{k_1\lambda_{lmn}}{\rho c_t}(t-t^*)}q_3(\boldsymbol{x}^*,t^*)\,\mathrm{d}t^*\,\mathrm{d}\mathcal{S} \tag{19}$$

where q_3 is the component of the heat density vector $\boldsymbol{q}$ in the thickness x_3 direction.

To illustrate pictorially the idea behind this approach, a snapshot of the deformed configuration of the wing impacted by a generic heat density vector $\boldsymbol{q}$ is presented in Fig. 2. From this figure, it becomes apparent how the heat flux absorbed by the wing can depend on its actual deformation and, as a result, the temperature field on the displacement vector. Finally, it is worth pointing out that the temperature in Eqs. (17) and (18) is a function of space and time by means of the actual displacement vector, even if the heat density vector is supposed to be constant in space and time, as it will be assumed later in the application.

Using Eqs. (17–19), the thermal moment in Eq. (5) expressed in terms of the vector of displacement unknowns is

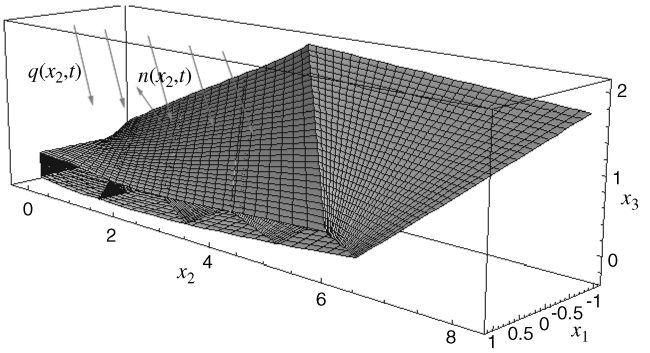

Fig. 2 Effect of the aeroelastic deformation of the wing structure on the evaluation of the temperature field.

$$\boldsymbol{c}(\boldsymbol{y},\boldsymbol{y}',x_2,t)=\sum_{m=0}^{\infty}\int_0^t \mathrm{U}(m,x_2,t-t^*)\int_0^L[\mathrm{U}_1(m,x_2^*,t^*)\boldsymbol{y}(x_2^*,t^*)+\mathrm{U}_{\mathbf{2}}(m,x_2^*,t^*)\boldsymbol{y}'(x_2^*,t^*)]\,\mathrm{d}x_2^*\,\mathrm{d}t^*+\boldsymbol{c}_3(t) \tag{20}$$

where $\boldsymbol{c}_3$ denotes the contribution to the thermal load vector provided by the term in Eq. (19), and U, U_1, and $\mathrm{U}_{\mathbf{2}}$ are three matrix operators whose definition can be deduced from the expression of the temperature field and are given by

$$\mathrm{U}(m,x_2^*,t-t^*)=\begin{bmatrix}1&0&0&0\\0&0&0&0\\0&0&0&0\\0&0&0&0\end{bmatrix}\sum_{l,n=0}^{\infty}\int_{-c/2}^{c/2}\int_{-H/2}^{H/2}x_3\hat{\boldsymbol{\alpha}}\frac{\phi_{lmn}(x_1,x_2^*,x_3)}{\rho c_t}e^{-\frac{k_1\lambda_{lmn}}{\rho c_t}(t-t^*)}\times\int_{-c/2}^{c/2}(-1)^n\cos\left[\frac{l\pi x_1^*}{c}\right]\mathrm{d}x_1^*\,\mathrm{d}x_3\,\mathrm{d}x_1 \tag{21}$$

$$\mathrm{U}_{\mathbf{1}}(m,x_2^*,t)=\begin{bmatrix}0&0&1&0\\0&0&0&0\\0&0&0&0\\0&0&0&0\end{bmatrix}q_1(t^*)\cos\left(\frac{m\pi x_2^*}{L}\right) \tag{22}$$

$$\mathrm{U}_{\mathbf{2}}(m,x_2^*,t)=\begin{bmatrix}0&0&0&-1\\0&0&0&0\\0&0&0&0\\0&0&0&0\end{bmatrix}q_2(t^*)\cos\left(\frac{m\pi x_2^*}{L}\right) \tag{23}$$

At this point, it should be recalled that due to the particular geometry of the wing, the thermal moment induced by the heat flux in the x_3 direction reduces to a function of time only, once the heat flux q_3 is assumed constant in space. Indeed, in the contribution to the temperature field T_3, the integrals of the eigenfunctions are all zero except for $l=m=0$, thus this term reduces to a function of x_3 and t only. The functional dependence on the coordinate x_3 is successively eliminated by the integration across the wing cross section of the thermal moment [Eq. (5)].

Therefore, the vector of thermomechanical loads appearing in Eq. (4) becomes

$$\boldsymbol{f}^T(\boldsymbol{y},\boldsymbol{y}',x_2,t)=\boldsymbol{c}'(\boldsymbol{y},\boldsymbol{y}',x_2,t)=\sum_{m=0}^{\infty}\int_0^t \mathrm{U}'(m,x_2,t-t^*)\int_0^L[\mathrm{U}_{\mathbf{1}}(m,x_2^*,t^*)\boldsymbol{y}(x_2^*,t^*)+\mathrm{U}_{\mathbf{2}}(m,x_2^*,t^*)\boldsymbol{y}'(x_2^*,t^*)]\,\mathrm{d}x_2^*\,\mathrm{d}t^* \tag{24}$$

Note that the displacement vector $\boldsymbol{y}$ appears in the previous expression under the integral sign. There is, indeed, a convolution between the thermal input and the displacement field. The consideration of this integral constitutes a significative part of the next section. Before proceeding further, it is remarkable to point out that in the solution of the aerothermoelastic problem, an important role will be played by the parameter B [5] representing the ratio t_T/t_M between the characteristic thermal time ($t_T=\rho c_t H^2/k_3$) and a characteristic mechanical time (for instance, the first natural bending period). As it is stated in [5], the dynamic coupling increases as B becomes smaller. On the other hand, as B becomes larger, the dynamic coupling disappears and the static solution alone remains valid.

IV. Solution Methodology

Following [12,19], the system of aerothermoelastic governing equations [Eq. (2)] with the associated boundary conditions [Eqs. (7) and (8)] can be reduced to a system of algebraic equations in the Laplace space and time domains, in which both the space and time

coordinates are converted to their Laplace counterparts. Indeed, applying the Laplace transform with respect to time to Eq. (2), and assuming zero initial conditions, one has

$$\mathrm{K}\tilde{\boldsymbol{y}}'' + \tilde{\mathrm{N}}(s,U)\tilde{\boldsymbol{y}}' + \tilde{\mathrm{Q}}(s,U)\tilde{\boldsymbol{y}} = \tilde{\boldsymbol{f}}^T(x_2,s) + \tilde{\boldsymbol{f}}^M(x_2,s) \tag{25}$$

where the tilde ($L_t[\bullet] \equiv \tilde{\bullet}$) denotes the Laplace transform with respect to time, s is the Laplace transform variable representing the time counterpart t of the physical space, and $\tilde{\mathrm{N}}$ and $\tilde{\mathrm{Q}}$ are two matrix operators which take into account the aerodynamic coupling and are given by

$$\tilde{\mathrm{N}}(s,U) = \mathrm{L} - \mathrm{C} - s\mathrm{D} - s\tilde{\varphi}\mathrm{G} \tag{26}$$

$$\tilde{\mathrm{Q}}(s,U) = \mathrm{N} + s^2(\mathrm{M} - \mathrm{A} - \tilde{\varphi}\mathrm{E}) - s(\mathrm{B} + \tilde{\varphi}\mathrm{F}) \tag{27}$$

where $\tilde{\varphi}$ is the Laplace transform of Wagner's function and it is given by

$$\tilde{\varphi} = L_t[\varphi(t)] = \frac{C(s)}{s} \tag{28}$$

where C is the extension on the Laplace domain of the Theodorsen function.

Similarly, performing the Laplace transform with respect to space, and recalling that the wing is considered to be clamped at the root cross section, one has

$$\hat{\tilde{\boldsymbol{y}}}(p,s) = [p^2\mathrm{K} + p\tilde{\mathrm{N}}(s,U_n) + \tilde{\mathrm{Q}}(s,U_n)]^{-1}[-\hat{\tilde{\boldsymbol{f}}}^T(p,s) - \hat{\tilde{\boldsymbol{f}}}^M(p,s) + \mathrm{K}\tilde{\boldsymbol{y}}'(0,s)] \tag{29}$$

where the overhat ($L_{x_2}[\bullet] \equiv \hat{\bullet}$) denotes the Laplace transform with respect to coordinate x_2, and p is the Laplace transform variable counterpart of x_2. It is useful to indicate at this point that the assumption of constant heat flux in space and time yields the matrix operators U_1 and U_2 to be independent of time, and thus reduces Eq. (24) to a convolution in time of U and the space vector $\boldsymbol{y}$ and its first derivative $\boldsymbol{y}'$.

In the following, we will not consider other loads than those produced by the heat inputs (i.e., we will assume $\boldsymbol{f}^M = 0$); thus, the thermal load vector, using Eq. (24) and assuming a constant heat flux in space and time, may be written as

$$\hat{\tilde{\boldsymbol{f}}}^T(p,s) = \sum_{m=0}^{\infty} p\hat{\tilde{\mathrm{U}}}(m,p,s)\int_0^L [\mathrm{U}_1(m,x_2^*)\tilde{\boldsymbol{y}}(x_2^*,s) + \mathrm{U}_2(m,x_2^*)\tilde{\boldsymbol{y}}'(x_2^*,s)]\,\mathrm{d}x_2^* \tag{30}$$

where it made use of the convolution theorem to perform time-Laplace transform of the time integral in Eq. (24). Denoting the first multiplicative term in Eq. (29) as

$$\hat{\tilde{\mathrm{H}}}(p,s,U) = [p^2\mathrm{K} + p\tilde{\mathrm{N}}(s,U) + \tilde{\mathrm{Q}}(s,U)]^{-1} \tag{31}$$

which can be regarded as the aeroelastic operator, and, using Eqs. (29) and (30), one may write the displacement vector for the particular problem of a heated wing in an incompressible flowfield [Eq. (29)] as

$$\hat{\tilde{\boldsymbol{y}}}(p,s) = \hat{\tilde{\mathrm{H}}}(p,s,U)\left\{-\sum_{m=0}^{\infty} p\hat{\tilde{\mathrm{U}}}(m,p,s)\int_0^L [\mathrm{U}_1(m,x_2^*)\tilde{\boldsymbol{y}}(x_2^*,s) + \mathrm{U}_2(m,x_2^*)\tilde{\boldsymbol{y}}'(x_2^*,s)]\,\mathrm{d}x_2^* + \mathrm{K}\tilde{\boldsymbol{y}}'(0,s)\right\} \tag{32}$$

Applying the inverse Laplace transform with respect to space to Eq. (32), one has

$$\tilde{\boldsymbol{y}}(x_2,s) = -\sum_{m=0}^{\infty}\int_0^{x_2} \tilde{\mathrm{H}}(\eta,s)\tilde{\mathrm{U}}'(m,x_2-\eta,s) \times \left[\int_0^L \mathrm{U}_1(m,x_2^*)\tilde{\boldsymbol{y}}(x_2^*,s)\,\mathrm{d}x_2^* + \int_0^L \mathrm{U}_2(m,x_2^*)\tilde{\boldsymbol{y}}'(x_2^*,s)\,\mathrm{d}x_2^*\right]\mathrm{d}\eta + \tilde{\mathrm{H}}(x_2,s,U)\mathrm{K}\tilde{\boldsymbol{y}}'(0,s) \tag{33}$$

Upon defining

$$\tilde{\boldsymbol{g}}(x_2,s) = -\int_0^{x_2} \tilde{\mathrm{H}}(\eta,s)\tilde{\mathrm{U}}(m,x_2-\eta,s)\,\mathrm{d}\eta \tag{34}$$

and differentiating Eq. (33) with respect to the spanwise coordinate x_2, one has

$$\tilde{\boldsymbol{y}}'(x_2,s) = \sum_{m=0}^{\infty} \tilde{\boldsymbol{g}}'(m,x_2,s)\left[\int_0^L \mathrm{U}_1(m,x_2^*)\tilde{\boldsymbol{y}}(x_2^*,s)\,\mathrm{d}x_2^* + \int_0^L \mathrm{U}_2(m,x_2^*)\tilde{\boldsymbol{y}}'(x_2^*,s)\,\mathrm{d}x_2^*\right] + \tilde{\mathrm{H}}'(x_2,s,U)\mathrm{K}\tilde{\boldsymbol{y}}'(0,s) \tag{35}$$

Thus, one may use the boundary condition at the tip [Eq. (8)], properly rewritten in the transformed Laplace time domain, to evaluate the unknown derivative $\tilde{\boldsymbol{y}}'(0,s)$ appearing in the previous equations. Indeed, substituting Eqs. (33) and (35) in Laplace transformed counterpart of Eq. (8), one has

$$\begin{aligned}
&\mathrm{R}\left\{\tilde{\mathrm{H}}'(L,s)\mathrm{K}\tilde{\boldsymbol{y}}'(0,s) + \sum_{m=0}^{\infty}\tilde{\boldsymbol{g}}'(m,L,s)\int_0^L [\mathrm{U}_1(m,x_2^*)\tilde{\boldsymbol{y}}(x_2^*,s) + \mathrm{U}_2(m,x_2^*)\tilde{\boldsymbol{y}}'(x_2^*,s)]\,\mathrm{d}x_2^*\right\} + \mathrm{S}\left\{\tilde{\mathrm{H}}(L,s)\mathrm{K}\tilde{\boldsymbol{y}}'(0,s)\right.\\
&\left. + \sum_{m=0}^{\infty}\tilde{\boldsymbol{g}}(m,L,s)\int_0^L [\mathrm{U}_1(m,x_2^*)\tilde{\boldsymbol{y}}(x_2^*,s) + \mathrm{U}_2(m,x_2^*)\tilde{\boldsymbol{y}}'(x_2^*,s)]\,\mathrm{d}x_2^*\right\}\\
&= \sum_{m=0}^{\infty}\tilde{\mathrm{U}}(m,L,s)\int_0^L [\mathrm{U}_1(m,x_2^*)\tilde{\boldsymbol{y}}(x_2^*,s) + \mathrm{U}_2(m,x_2^*)\tilde{\boldsymbol{y}}'(x_2^*,s)]\,\mathrm{d}x_2^* + \tilde{\boldsymbol{c}}_3(s)
\end{aligned} \tag{36}$$

thus, the vector of unknown boundary conditions $\tilde{\boldsymbol{y}}'(0,s)$ may be written as

$$\begin{aligned}
\tilde{\boldsymbol{y}}'(0,s) = &-[\mathrm{R}\tilde{\mathrm{H}}'(L,s)\mathrm{K} + \mathrm{S}\tilde{\mathrm{H}}(L,s)\mathrm{K}]^{-1}\left\{\textstyle\sum_{m=0}^{\infty}[\mathrm{R}\tilde{\boldsymbol{g}}'(m,L,s) + \mathrm{S}\tilde{\boldsymbol{g}}(m,L,s) - \tilde{\mathrm{U}}(m,L,s)]\int_0^L [\mathrm{U}_1(m,x_2^*)\tilde{\boldsymbol{y}}(x_2^*,s)\right.\\
&\left. + \mathrm{U}_2(m,x_2^*)\tilde{\boldsymbol{y}}'(x_2^*,s)]\,\mathrm{d}x_2^* + \tilde{\boldsymbol{c}}_3(s)\right\}
\end{aligned} \tag{37}$$

Introducing the following definitions

$$\tilde{\mathrm{W}}(s) = [\mathrm{R}\tilde{\mathrm{H}}'(L,s)\mathrm{K} + \mathrm{S}\tilde{\mathrm{H}}(L,s)\mathrm{K}] \tag{38}$$

$$\tilde{\mathrm{V}}(m,s) = -[\mathrm{R}\tilde{\boldsymbol{g}}'(m,L,s) + \mathrm{S}\tilde{\boldsymbol{g}}(m,L,s) - \tilde{\mathrm{U}}(m,L,s)] \tag{39}$$

and substituting them in Eqs. (33) and (37), one may obtain the closed form solution of the problem in the double transformed Laplace space-time domain

$$\tilde{\boldsymbol{y}}(x_2,s)=\tilde{\mathrm{H}}(x_2,s)\mathrm{K}\Big\{\tilde{\mathrm{W}}^{-1}(s)\sum_{m=0}^{\infty}\tilde{\mathrm{V}}(m,s)\int_0^L[\mathrm{U}_1(m,x_2^*)\tilde{\boldsymbol{y}}(x_2^*,s)+\mathrm{U}_2(m,x_2^*)\tilde{\boldsymbol{y}}'(x_2^*,s)]\,\mathrm{d}x_2^*+\tilde{\mathrm{W}}^{-1}(s)\tilde{\boldsymbol{c}}_3(s)\Big\}+\sum_{m=0}^{\infty}\tilde{\boldsymbol{g}}(m,x_2,s)\times\int_0^L[\mathrm{U}_1(m,x_2^*)\tilde{\boldsymbol{y}}(x_2^*,s)+\mathrm{U}_2(m,x_2^*)\tilde{\boldsymbol{y}}'(x_2^*,s)]\,\mathrm{d}x_2^*$$
$$=\sum_{m=0}^{\infty}[\tilde{\mathrm{H}}(x_2,s)\mathrm{K}\tilde{\mathrm{W}}^{-1}(s)\tilde{\mathrm{V}}(m,s)+\tilde{\boldsymbol{g}}(m,x_2,s)]\times\int_0^L[\mathrm{U}_1(m,x_2^*)\tilde{\boldsymbol{y}}(x_2^*,s)+\mathrm{U}_2(m,x_2^*)\tilde{\boldsymbol{y}}'(x_2^*,s)]\,\mathrm{d}x_2^*+\tilde{\mathrm{H}}(x_2,s)\mathrm{K}\tilde{\mathrm{W}}^{-1}(s)\tilde{\boldsymbol{c}}_3(s) \tag{40}$$

One should remark that the displacement vector $\boldsymbol{y}$ appears not only in the left-hand side of Eq. (40) but also in its right-hand side under the integral sign.

Therefore, it is apparent that to solve this integral equation, one should employ a numerical scheme, consisting of either the discretization of the integral, or of an approximation of the vector of unknowns on a certain functional basis. In this paper, a numerical discretization of the integral has been used to solve the coupled aerothermoelastic stability of the wing model. Nonetheless, a Galerkin approach has also been applied in the first elementary application. This has been done only to validate the model, by comparing the obtained predictions with those available in the literature.

Specifically, the integrals in Eq. (40) may be discretized as

$$\int_0^L \mathrm{U}_1(m,x_2^*)\tilde{\boldsymbol{y}}(x_2^*,s)\,\mathrm{d}x_2^*\simeq\sum_{k=0}^{N-1}\mathrm{U}_1(m,x_{2k})\tilde{\boldsymbol{y}}(x_{2k},s)\Delta x_2 \tag{41}$$

$$\int_0^L \mathrm{U}_2(m,x_2^*)\tilde{\boldsymbol{y}}'(x_2^*,s)\,\mathrm{d}x_2^*\simeq\mathrm{U}_2(m,L)\tilde{\boldsymbol{y}}(L,s)-\sum_{k=0}^{N-1}\mathrm{U}_2'(m,x_{2k})\tilde{\boldsymbol{y}}(x_{2k},s)\Delta x_2 \tag{42}$$

where N is the number of points on which the integral has been discretized and Δx_2 is the step in x_2

$$N=\frac{L}{\Delta x_2} \tag{43}$$

and where the evident relationship

$$\int_0^L \mathrm{U}_2(m,x_2^*)\tilde{\boldsymbol{y}}'(x_2^*,s)\,\mathrm{d}x_2^*=[\mathrm{U}_2(m,x_2^*)\tilde{\boldsymbol{y}}(x_2^*,s)]_0^L-\int_0^L\mathrm{U}_2'(m,x_2^*)\tilde{\boldsymbol{y}}(x_2^*,s)\Delta x_2^*=\mathrm{U}_2(m,L)\tilde{\boldsymbol{y}}(L,s)-\int_0^L\mathrm{U}_2'(m,x_2^*)\tilde{\boldsymbol{y}}(x_2^*,s)\Delta x_2^*$$

was used, in which the boundary condition at the root $\tilde{\boldsymbol{y}}(0,s)=0$ was imposed.

Hence, Eq. (40) may be rewritten

$$\tilde{\boldsymbol{y}}(x_{2k},s)=\sum_{m=0}^{\infty}[\tilde{\mathrm{H}}(x_{2k},s)\mathrm{K}\tilde{\mathrm{W}}^{-1}(s)\tilde{\mathrm{V}}(m,s)+\tilde{\boldsymbol{g}}(m,x_{2k},s)]\Big[\sum_{k=0}^{N-1}\mathrm{U}_1(m,x_{2k})\tilde{\boldsymbol{y}}(x_{2k},s)\Delta x_{2k}+\mathrm{U}_2(m,L)\tilde{\boldsymbol{y}}(L,s)-\sum_{k=0}^{N-1}\mathrm{U}_2'(m,x_{2k})\tilde{\boldsymbol{y}}(x_{2k},s)\Delta x_{2k}\Big]+\tilde{\mathrm{H}}(x_{2k},s)\mathrm{K}\tilde{\mathrm{W}}^{-1}(s)\tilde{\boldsymbol{c}}_3(s) \tag{44}$$

Introducing the discrete vector of unknowns $\tilde{\boldsymbol{Y}}(s)$

$$\tilde{\boldsymbol{Y}}(s)=\{\tilde{\boldsymbol{y}}(x_{20},s),\tilde{\boldsymbol{y}}(x_{21},s),\ldots,\tilde{\boldsymbol{y}}(x_{2N},s)\}^T \tag{45}$$

and defining the following matrix operators $\tilde{\mathrm{Z}}$, C_1, C_2, C_3, A of dimension $4N\times 4N$ each

$$\tilde{\mathrm{Z}}(m,s)=\begin{bmatrix}\ddots & & \\ & \tilde{\mathrm{H}}(x_{2k},s)\mathrm{K}\tilde{\mathrm{W}}^{-1}(s)\tilde{\mathrm{V}}(m,s)+\tilde{\boldsymbol{g}}(m,x_{2k},s) & \\ & & \ddots\end{bmatrix} \tag{46}$$

$$\mathrm{C}_1(m)=\begin{bmatrix}\mathrm{U}_1(m,x_{20}) & \mathrm{U}_1(m,x_{2k}) & \mathrm{U}_1(m,x_{2(N-1)})\\ \vdots & \vdots & \vdots\\ \mathrm{U}_1(m,x_{20}) & \mathrm{U}_1(m,x_{2k}) & \mathrm{U}_1(m,x_{2(N-1)})\end{bmatrix} \tag{47}$$

$$\mathrm{C}_2(m)=\begin{bmatrix}0 & \ldots & \mathrm{U}_2(m,L)\\ \vdots & \vdots & \vdots\\ 0 & \ldots & \mathrm{U}_2(m,L)\end{bmatrix} \tag{48}$$

$$\mathrm{C}_3(m)=\begin{bmatrix}\mathrm{U}_2'(m,x_{20}) & \mathrm{U}_2'(m,x_{2k}) & \mathrm{U}_2'(m,x_{2(N-1)})\\ \vdots & \vdots & \vdots\\ \mathrm{U}_2'(m,x_{20}) & \mathrm{U}_2'(m,x_{2k}) & \mathrm{U}_2'(m,x_{2(N-1)})\end{bmatrix} \tag{49}$$

$$\tilde{\mathrm{A}}(s)=\begin{bmatrix}\ddots & & \\ & \tilde{\mathrm{H}}(x_{2k},s)\mathrm{K}\tilde{\mathrm{W}}^{-1}(s) & \\ & & \ddots\end{bmatrix} \tag{50}$$

Equation (44) becomes

$$\Big\{\mathrm{I}-\sum_{m=0}^{\infty}\tilde{\mathrm{Z}}(m,s)[\mathrm{C}_1(m)\Delta x_2-\mathrm{C}_2(m)+\mathrm{C}_3(m)\Delta x_2]\Big\}\tilde{\boldsymbol{Y}}(s)=\tilde{\mathrm{A}}(s)\tilde{\mathrm{F}}_3^T(s) \tag{51}$$

Finally, from the previous equation, one obtains

$$\tilde{\boldsymbol{Y}}(s)=\Big\{\mathrm{I}-\sum_{m=0}^{\infty}\tilde{\mathrm{Z}}(m,s)[\mathrm{C}_1(m)\Delta x_2-\mathrm{C}_2(m)+\mathrm{C}_3(m)\Delta x_2]\Big\}^{-1}\tilde{\mathrm{A}}(s)\tilde{\mathrm{F}}_3^T(s) \tag{52}$$

One should notice that by discarding the components of the heat flux in the chordwise and spanwise directions, which implies that no thermomechanical coupling is involved, the previous equation provides the aeroelastic response in the Laplace transformed time domain, due to the application of an external heat flux in the thickness direction [12]. Finally, note that the evaluation of the roots of the determinant of the matrix operator in brackets in Eq. (52) are the poles of the considered aerothermoelastic system. The evaluation of these poles at different flight speeds and different heat fluxes permits the determination of the domains of aerothermoelastic stability/instability of the wing. This analysis will be presented in the following section, after a comparative analysis with some results available in the literature.

V. Numerical Results

Goland's wing structural model [25] has been considered as a reference configuration for the validation of the present model. Corresponding to it, the following geometrical and dynamic characteristics have been assumed

$$\begin{aligned} &L = 6.096 \text{ m} \qquad c = 1.8288 \text{ m} \qquad a = -1/3 \\ &x_{\text{cg}} = 0.4c \qquad \omega_{1,b} = 50 \text{ rad/s} \qquad \omega_{1,t} = 87 \text{ rad/s} \end{aligned} \tag{53}$$

where L is the midspan, c is the chord measured normally to the trailing edge, a is the nondimensional offset (with respect to the midchord) between the aerodynamic center and the elastic center, and x_{cg} is the distance between the center of gravity and the elastic center of the wing, whereas ω_{1b} and ω_{1t} are, respectively, the first uncoupled bending and torsion angular frequencies of the wing. In the following, as a validation of results obtained in the available literature, a static/dynamic stability analysis of the thermoelastic model is presented. Then, a complete aerothermoelastic analysis is performed, and the corresponding aerothermoelastic flutter boundaries are obtained.

A. Validation of the Thermoelastic Model

As already mentioned in the Introduction, only a few results are available in literature related to the thermoelastic dynamic stability of beams (see, for instance, [7–9]). Moreover, one should remark that those results are approximated in the sense that they have been obtained using an ab initio approximate expression of the temperature field and a collocated or Galerkin approach. Nonetheless, using the mathematical model developed in the previous section, discarding the aerodynamic forces, and introducing a structural damping $\zeta = 0.001$, one may study the root locus relative to the first two roots (bending and torsion natural frequencies) as a function of the components in the three directions of the impacting heat flux. Moreover, as illustrated in the previous section, the effect of the heat flux in the thickness direction q_3 does not induce, in the linear approximation, any thermoelastic coupling, but it is responsible only for an equivalent mechanical load, which cannot modify the elastic stability of the wing model [12]. On the other hand, the contributions to the thermal moment of q_1 and q_2 induce a thermomechanical coupling that can modify the elastic stability [see Eqs. (24) and (52)]. This effect has been already pointed out in [7,9,26–28]. In particular, in [27], it was observed that a cantilevered flexural beam subjected to radiant heat is dynamically stable if $q_2 < 0$ (i.e., if the heat input is directed from the tip to the root of the beam) and it is dynamically unstable (thermal flutter) if $q_2 > 0$ (i.e., if the heat input is directed from the root to the tip in the positive x_2 direction). We have not only obtained the same dynamic behavior, but we have also found that the model becomes statically unstable for a certain value of $q_2 < 0$. The roots loci of the system are presented in Figs. 3–5. In these figures, the lower frequency refers to the bending natural frequency, whereas the higher refers to the torsional frequency. It is worth pointing out that the results obtained are qualitatively in complete agreement with those reported in [7,9]. Indeed, the different direction of the heat flux, namely, from wing root to wing tip, or from the leading to the trailing edge, may induce different dynamic behavior for the stability: this result is motivated by the lack of symmetry in the wing span direction because of the boundary conditions and by the fact that the induced thermal fields given by the integral Eqs. (17) and (18) are linear functions of the heat flux components. Moreover, in Fig. 6, a map of the stability boundary for this particular wing model is supplied. The abscissa in Fig. 6 represents the amplitude (with sign) of the component of the heat density vector in the wing span direction (q_2), whereas the ordinate axis represents the amplitude (with sign) of the component of the heat density vector in the chordwise direction (q_1). The combinations of the two components of heat flux vector that yield a stable condition are identified with a star-shaped marker, whereas the unstable combinations are identified with a dot marker.

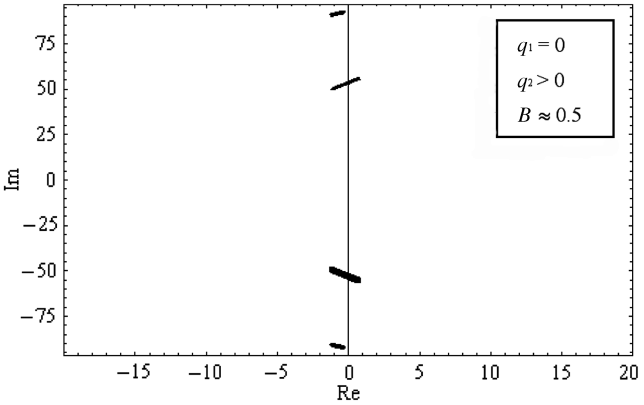

a) $q_2>0$

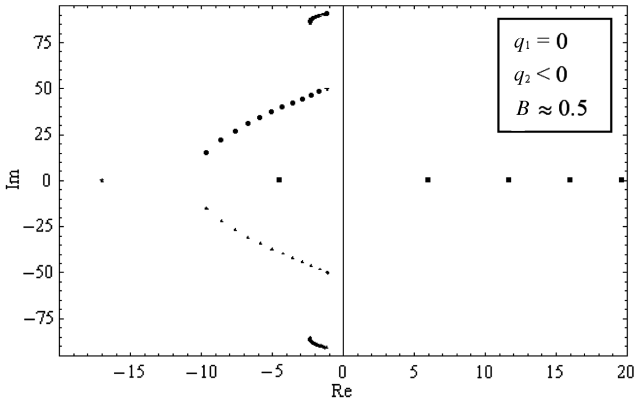

b) $q_2<0$

Fig. 3 Root locus of the thermoelastic model with $q_1 = 0$.

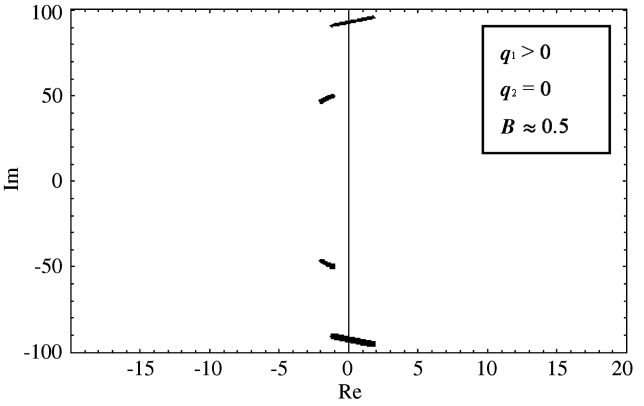

a) $q_1>0$

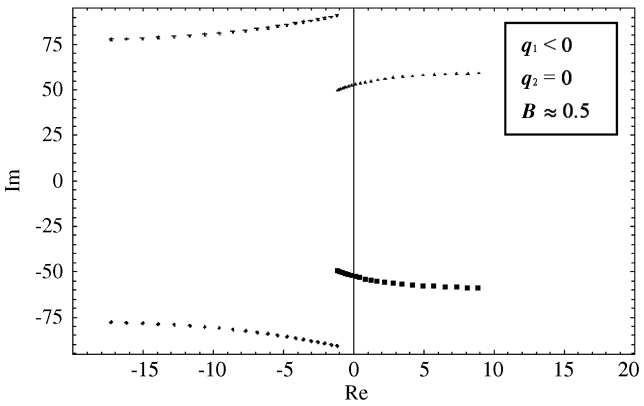

b) $q_1<0$

Fig. 4 Root locus of the thermoelastic model with $q_2 = 0$.

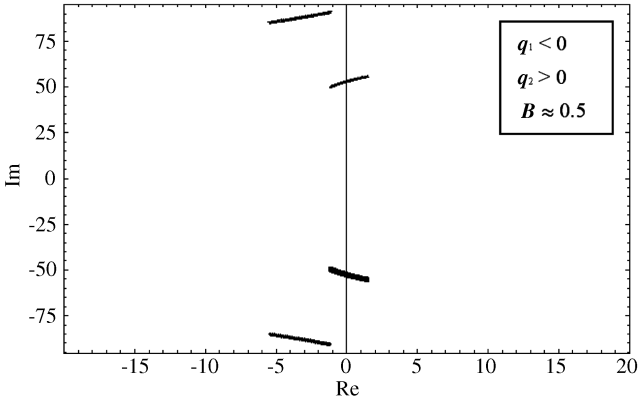

a) $q_2>0$

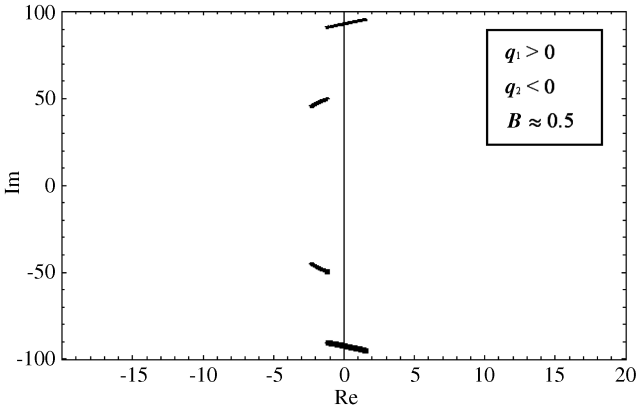

b) $q_2<0$

Fig. 5 Root locus of the thermoelastic model with $q_1 = -q_2$.

B. Aerothermoelastic Analysis

In this section, an exact approach has been employed to solve the previously defined initial boundary value problem. In particular, Eq. (52) has been used directly to obtain the static/dynamic stability boundaries of Goland's wing model [25,29] with warping restraint included, for different combinations of the heat density vector components (i.e., for different directions of the perturbing heat density vector). The methodology adopted, based on the use of a double Laplace transform, was originally developed in [30] to solve the static aeroelastic response, then employed in [13,31] to determine the flutter and divergence speed of swept composite wing structure,

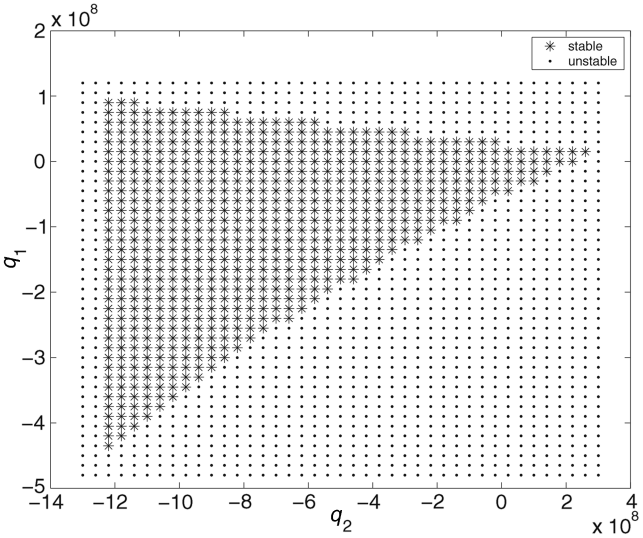

Fig. 6 Thermoelastic stability surface.

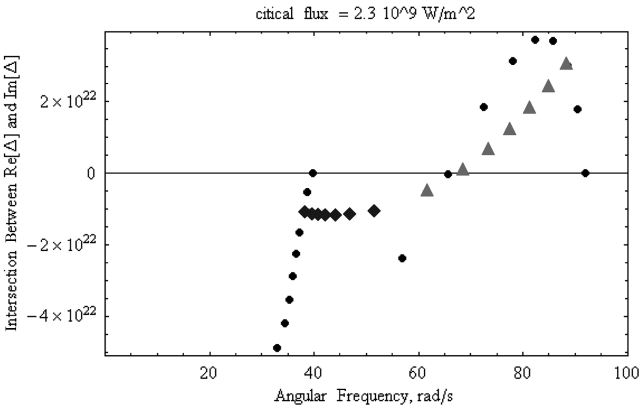

Fig. 7 Thermal effect on aeroelastic stability.

and in [19,20] to solve the aerothermoelastic dynamic response of the structure; finally, in this paper, it has been extended to the solution of an arbitrary dynamic aerothermoelastic coupled response.

In particular, Fig. 7 represents an example on how the present model can be used to extract important information regarding the aerothermoelastic stability of a composite wing impacted by a heat flux (generated, for instance, by a laser beam). Indeed, from Fig. 7 it appears that the effect of the external heating can influence the aeroelastic stability of the considered wing model. It shows the intersections of the real and imaginary parts of the determinant of the aerothermoelastic operator [see Eq. (52)] evaluated at various flight speeds and heat flux amplitudes. Indeed, according to [12,25] these intersections can be used as a root locus with the flight speed as a device or, as in this case, with the amplitude of the impacting heat flux as a parameter. In particular, in Fig. 7, the circular markers identify the root locus (in the restricted frequency range considered)

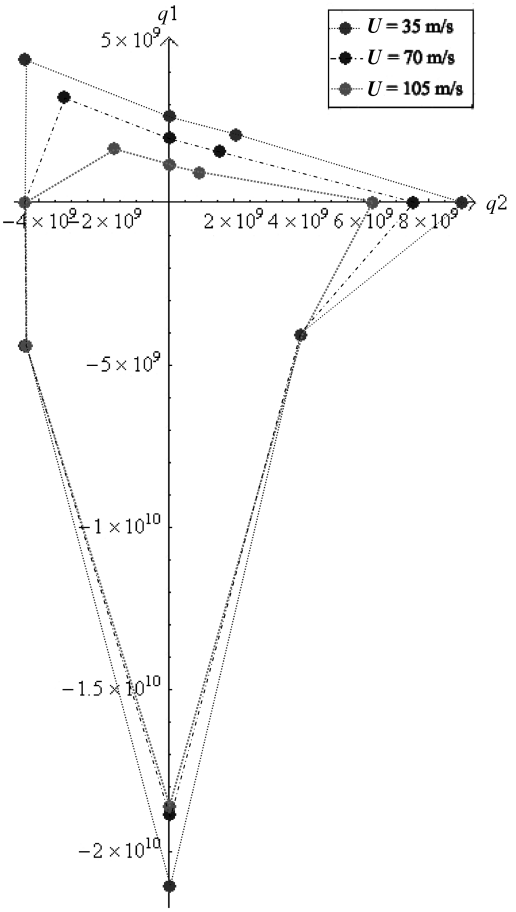

Fig. 8 Aerothermoelastic stability boundaries.

using the flight speed as parameter varying from 0 to 160 m/s. In this regard, it is worth noting that when an intersection occurs at the horizontal axis, this means that a dynamic unstable condition by flutter occurs (in this case, this happens at $U_{\text{Flutter}} = 139.6$ m/s and $\omega_{\text{Flutter}} = 65.71$ rad/s). On the other hand, the triangular markers identify the root locus using the heat flux amplitude as a parameter varying from 0 to 10^{10} W/m^2 and keeping a flight speed of $U = 40$ m/s. In this case, it has been found that a heat flux of 2.310^8 W/m^2 is critical for this system because it leads to an unstable condition on the torsional mode.

Moreover, Fig. 8 shows the stability surface obtained at a flight speed of 35, 70, and 105 m/s (respectively represented by gray, black, and light gray markers). In particular, in this figure, the component of the heat flux in the spanwise direction is represented on the horizontal axis (with a positive sign if the flux is from the root to the tip of the wing, with a negative sign in the opposite case), whereas the chordwise heat flux has been placed on the vertical axis (with a positive sign if the flux is from the leading edge to the trailing edge of the wing, or a negative sign in the opposite case). It is worth pointing out that, in contrast with the thermoelastic case (Fig. 6), here, the stability surface manifests a pronounced asymmetry with respect to the horizontal axis, due to the stabilizing effect of the aerodynamics. Moreover, the more interesting combinations of the thermal flux with applications in the aerospace and aeronautic fields are as follows: chordwise flux with direction from the leading edge to the trailing edge (corresponding to the case of the rectangular wing), and spanwise flux with a transverse component from the root to the tip of the wing (corresponding to the case of the swept wing). It has been found that this combination of heat flux is the most critical for the system. Other results concerning the aerothermoelastic response of the single-layered, uniform, rectangular swept wing has been found. In particular, the effects of flight speed (Fig. 8), the thermal conductivity anisotropy (Fig. 9), and the ratio of the characteristic thermal time to the natural period of vibration (Fig. 10) have been analyzed, indicating only a few points of instability, similar to the thermoelastic case previously studied (see Fig. 6). Concerning the effect of the flight speed, Fig. 8 shows three different stability domains obtained at three different flight speeds. In particular, one should notice that the domain of stability is reduced when the flight speed is increased. This behavior is due to the fact that the stability boundary is primarily governed by the aeroelastic coupling, and that the thermoelastic coupling can only worsen the scenario determined by the aeroelastic coupling (Fig. 7). Clearly, for a flight speed greater than the flutter speed (i.e., 140 m/s), the wing is unstable for any heat flux.

To evaluate the effect of the anisotropic thermal conductivity on the stability surface, Fig. 9 shows the stability boundaries, corresponding to a certain flight speed and a fixed thermal time to mechanical time ratio B. Specifically, the stability boundaries of the reference configuration (isotropic case $k_1 = k_2 = k_3$) are compared with those relevant to a transversely isotropic model ($k_1 = k_2 \neq k_3$). As in the pyrolytic graphite, the transverse thermal conductivity coefficient is about one-third of that in the plane of isotropy [32], and so we considered $k_3 = k_1/3$. In particular, Fig. 9 shows that the reduction of k_3 induces a worsening in the thermoelastic stability of

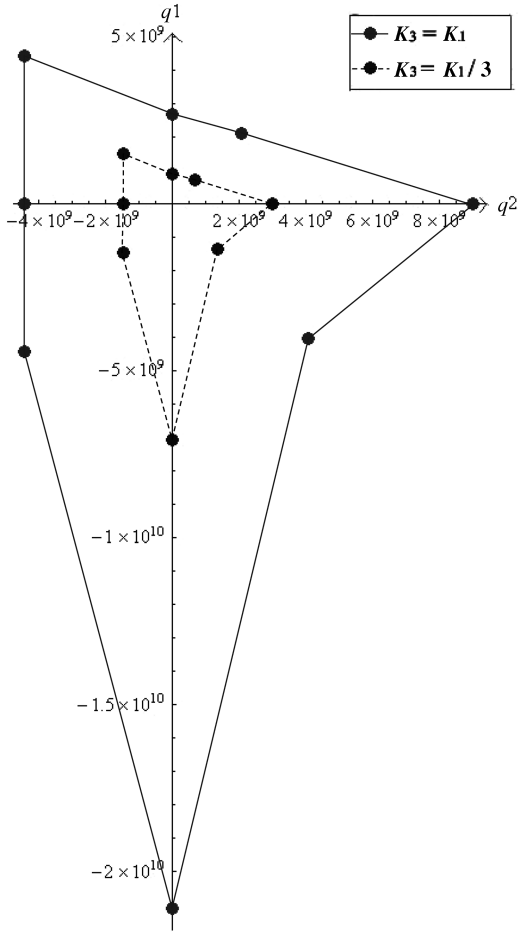

Fig. 9 Effect of thermal conductivity ratio of the constituent material on the aerothermoelastic stability boundaries.

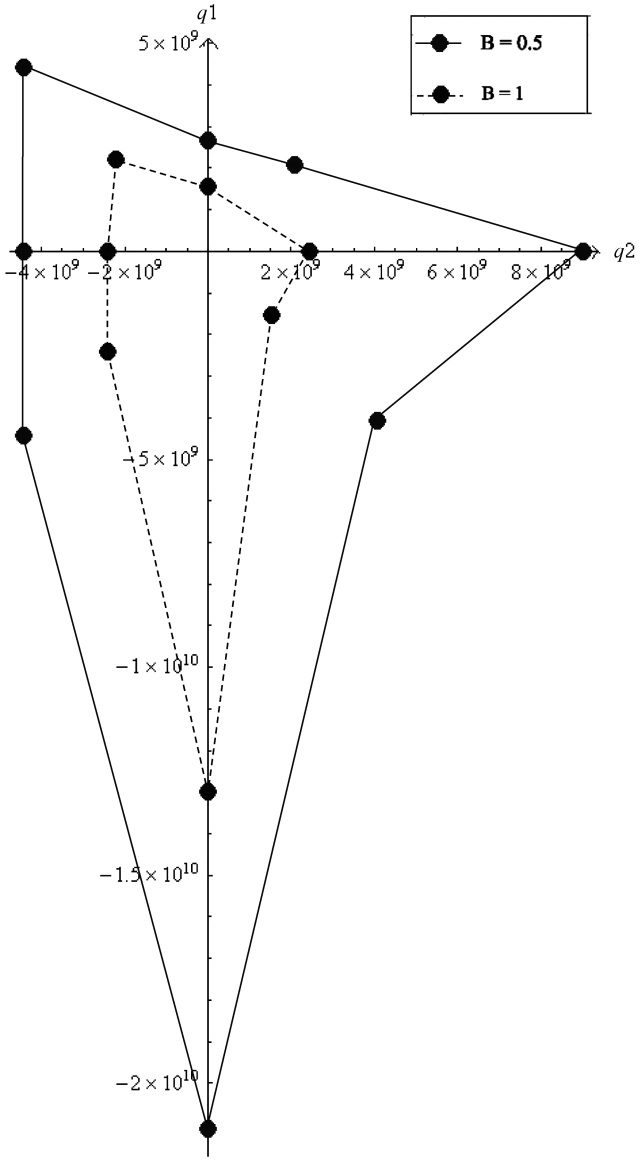

Fig. 10 Effect of the ratio of the characteristic thermal time to the natural period of vibration on boundaries of stability.

the model. To understand this result, consider that a reduction in the thermal conductivity across the wing thickness is equivalent in the model to an increase of the in-plane thermal conductivity. As a result, the thermoelastic feedback granted by the in-plane components of the temperature field (T_1 and T_2) would be increased and, consequently, the critical fluxes in the plane would decrease as represented in Fig. 9.

Finally, Fig. 10 shows two different stability surfaces obtained at two different ratios of the characteristic thermal time to the natural period of vibration B. The variation of this parameter has been obtained by a change of the thermal capacity of the structure. For $B \to 1$, the area of the stability surface decreases in agreement with that found in [5].

VI. Conclusions

In this paper, an exact aerothermoelastic analysis of swept wings featuring nonclassical structural effects and impacted by a heat flux vector was presented. The aerothermoelastic model is coupled in the sense that the thermal loads are coupled with the structural deformations in a similar way to what is usually done in the aeroelasticity discipline. The theoretical model was completely developed and the exact analytical solution was obtained using a double Laplace transform technique. Results concerning the thermoelastic and aerothermoelastic models are presented and compared with those available in the literature. As a natural development of the present model, the thermal and the unsteady aerodynamic field are considered to be coupled and, in this context, the problems of aerothermoelastic instability and response are addressed.

References

[1] Thuruthimattam, B. J., Friedmann, P. P., McNamara, J. J., and Powell, K., "Modeling Approaches to Hypersonic Aerothermoelasticity with Applications to Reusable Launch Vehicles," *44th AIAA/ASME/ASCE/AHS/ASC Structures, Structural Dynamics & Materials Conference*, AIAA Paper 2003-1967, 2003.

[2] Friedmann, P., McNamara, J., Thuruthimattam, B., and Nydick, I., "Aeroelastic Analysis of Hypersonic Vehicles," *Journal of Fluids and Structures*, Vol. 19, No. 5, 2004, pp. 681–712. doi:10.1016/j.jfluidstructs.2004.04.003

[3] McNamara, J. J., Thuruthimattam, B. J., Friedmann, P. P., and Powell, K., "Hypersonic Aerothermoelastic Studies for Reusable Launch Vehicles," *45th AIAA/ASME/ASCE/AHS/ASC Structures, Structural Dynamics & Materials Conference*, AIAA Paper 2004-1590, 2004.

[4] Thuruthimattam, B. J., Friedmann, P. P., McNamara, J. J., Powell, K. G., and Bartels, R. E., "Computational Study of Vehicle Aeroelastic and Aerothermoelastic Behavior in Hypersonic Flow," *CEAS/AIAA/DGLR International Forum on Aeroelasticity and Structural Dynamics*, AIAA Paper 200, 2005.

[5] Boley, B. A., and Weiner, J. H., *Theory of Thermal Stresses*, Wiley, New York, 1960.

[6] Augusti, G., "Instability of Struts Subject to Radiant Heat," *Meccanica*, Vol. 3, No. 3, 1968, pp. 167–176. doi:10.1007/BF02129249

[7] Yu, Y., "Thermally Induced Vibrations and Flutter of a Flexible Boom," *Journal of Spacecraft and Rockets*, Vol. 6, No. 8, 1969, pp. 902–910.

[8] Manolis, G., and Beskos, D., "Thermally Induced Vibrations of Beam Structures," *Computer Methods in Applied Mechanics and Engineering*, Vol. 21, No. 3, 1980, pp. 337–355. doi:10.1016/0045-7825(80)90101-2

[9] Thornton, E. A., *Thermal Structures for Aerospace Applications*, AIAA, Reston, VA, 1996.

[10] Blandino, J. R., and Thornton, E., "Thermally Induced Vibration of an Internally Heated Beam," *Journal of Vibration and Acoustics*, Vol. 123, No. 1, 2001, pp. 67–75. doi:10.1115/1.1320446

[11] Garrick, I. E., "Survey of Aerothermoelasticity," *Aerospace Engineering*, Vol. 22, No. 1, 1963, pp. 140–147.

[12] Polli, G. M., Librescu, L., and Mastroddi, F., "Aeroelastic Response of Composite Aircraft Swept Wings Impacted by a Laser Beam," *45th AIAA/ASME/ASCE/AHS/ASC Structures, Structural Dynamics & Materials Conference*, AIAA Paper 2004-2046, 2004.

[13] Karpouzian, G., and Librescu, L., "Comprehensive Model of Anisotropic Composite Aircraft Wings Suitable for Aeroelastic Analyses," *Journal of Aircraft*, Vol. 31, No. 3, 1994, pp. 703–712.

[14] Gern, F. H., and Librescu, L., "Static and Dynamic Aeroelasticity of Advanced Aircraft Wings Carrying External Stores," *AIAA Journal*, Vol. 36, No. 7, 1998, pp. 1121–1129.

[15] Garber, A. M., Pyrolytic Materials for Thermal Protection Systems, *Aerospace Engineering*, Vol. 22, No. 1, Jan. 1963, pp. 126–137.

[16] Nolan, E. J., and Scala, S. M., "Aerothermodynamic Behavior of Pyrolytic Graphite During Sustained Hypersonic Flight," *ARS Journal*, Vol. 32, No. 1, Jan. 1962, pp. 26–35.

[17] Fung, Y. C., *Introduction to the Theory of Aeroelasticity*, Dover, New York, 1969.

[18] Bisplinghoff, R. L., and Ashley, H., *Principles of Aeroelasticity*, Wiley, New York, 1962.

[19] Polli, G. M., "Structural Modeling for Aerothermoelastic Analysis and Control," Ph.D. Thesis, School of Aerospace Engineering, Univ. of Rome "La Sapienza," 2005.

[20] Polli, G. M., Librescu, L., and Mastroddi, F., "Aeroelastic Response of Composite Aircraft Swept Wings Impacted by a Laser Beam," *AIAA Journal*, Vol. 44, No. 2, 2006, pp. 382–391.

[21] Carslaw, H. S., and Jaeger, J. C., *Conduction of Heat in Solids*, Oxford Univ. Press, Oxford, 1959.

[22] Wei, Z. G., and Batra, R. C., "Deformations of an Axially Loaded Thermoviscoplastic Bar Due to Laser Heating," *Journal of Thermal Stresses*, Vol. 26, No. 7, 2003, pp. 701–712. doi:10.1080/713855993

[23] Arias, I., and Achenbach, J. D., "Thermoelastic Generation of Ultrasound by Line-Focused Laser Irradiation," *International Journal of Solids and Structures*, Vol. 40, No. 25, 2003, pp. 6917–6935. doi:10.1016/S0020-7683(03)00345-7

[24] Carlson, D. E., "Linear Thermoelasticity," *Encyclopedia of Physics*, Vol. 6a/2, edited by C. Truesdell, Springer–Verlag, Berlin, 1972, pp. 297–345.

[25] Goland, M., "Flutter of a Uniform Cantilever Wing," *Journal of Applied Mechanics*, Vol. 12, No. 4, 1945, pp. A197–A208.

[26] Augusti, G., "Comment on Thermally Induced Vibrations and Flutter of a Flexible Boom," *Journal of Spacecraft and Rockets*, Vol. 8, No. 2, 1971, pp. 204–208.

[27] Yu, Y. Y., "Reply by Author to P. F. Jordan and G. Augusti and New Results of Two-Modes Approximation Based on a Rigorous Analysis of Thermal Bending Flutter of a Flexible Boom," *Journal of Spacecraft and Rockets*, Vol. 8, No. 2, 1971, pp. 205–208.

[28] Givoli, D., and Rand, O., "Thermoelastic Analysis of Space Structures in Periodic Motion," *Journal of Spacecraft and Rockets*, Vol. 28, No. 4, 1991, pp. 457–464.

[29] Goland, M., and Luke, Y. L., "Flutter of a Uniform Wing with Tip Weights," *Journal of Applied Mechanics*, Vol. 15, No. 1, 1948, pp. 13–20.

[30] Librescu, L., and Thangjitham, S., "Analytical Studies on Static Aeroelastic Behavior of Forward-Swept Composite Wing Structures," *Journal of Aircraft*, Vol. 28, No. 2, 1991, pp. 151–157.

[31] Karpouzian, G., and Librescu, L., "Nonclassical Effects on Divergence and Flutter of Anisotropic Swept Aircraft Wings," *AIAA Journal*, Vol. 34, No. 4, 1996, pp. 768–794.

[32] Gebhardt, J. J., and Berry, J. M., "Mechanical Properties of Pyrolytic Graphite," *AIAA Journal*, Vol. 3, No. 2, Feb. 1965, pp. 302–308.

F. Pai
Associate Editor